Check for updates

Original Article

Rapid prototyped porous nickel–titanium scaffolds as bone substitutes

Journal of Tissue Engineering
Volume 5: 1–14
© The Author(s) 2014
DOI: 10.1177/2041731414540674
tej.sagepub.com
SAGE

Waldemar Hoffmann[1,2], Therese Bormann[2,3], Antonella Rossi[4,5], Bert Müller[3], Ralf Schumacher[2], Ivan Martin[1], Michael de Wild[2] and David Wendt[1]

Abstract

While calcium phosphate–based ceramics are currently the most widely used materials in bone repair, they generally lack tensile strength for initial load bearing. Bulk titanium is the gold standard of metallic implant materials, but does not match the mechanical properties of the surrounding bone, potentially leading to problems of fixation and bone resorption. As an alternative, nickel–titanium alloys possess a unique combination of mechanical properties including a relatively low elastic modulus, pseudoelasticity, and high damping capacity, matching the properties of bone better than any other metallic material. With the ultimate goal of fabricating porous implants for spinal, orthopedic and dental applications, nickel–titanium substrates were fabricated by means of selective laser melting. The response of human mesenchymal stromal cells to the nickel–titanium substrates was compared to mesenchymal stromal cells cultured on clinically used titanium. Selective laser melted titanium as well as surface-treated nickel–titanium and titanium served as controls. Mesenchymal stromal cells had similar proliferation rates when cultured on selective laser melted nickel–titanium, clinically used titanium, or controls. Osteogenic differentiation was similar for mesenchymal stromal cells cultured on the selected materials, as indicated by similar gene expression levels of bone sialoprotein and osteocalcin. Mesenchymal stromal cells seeded and cultured on porous three-dimensional selective laser melted nickel–titanium scaffolds homogeneously colonized the scaffold, and following osteogenic induction, filled the scaffold's pore volume with extracellular matrix. The combination of bone-related mechanical properties of selective laser melted nickel–titanium with its cytocompatibility and support of osteogenic differentiation of mesenchymal stromal cells highlights its potential as a superior bone substitute as compared to clinically used titanium.

Keywords

Bone tissue engineering, osteogenic differentiation, nickel–titanium, scaffold, selective laser melting

Received: 7 April 2014; accepted: 22 May 2014

Introduction

The most widely used scaffold materials for bone tissue engineering applications are calcium phosphate ceramics (e.g., hydroxyapatite and tricalcium phosphate) due to their osteoinductive and osteoconductive properties.[1–4] However, these materials generally lack the tensile strength required for initial load bearing and primary stability and, as bulk material, do not match the mechanical properties of the surrounding bone, limiting their application to non-load-bearing situations or requiring long periods of immobilization during bone healing.

As an alternative to ceramics, metals have been used for prostheses in orthopedics and orthodontics for decades due

[1]Departments of Biomedicine and Surgery, University Hospital Basel, Basel, Switzerland
[2]University of Applied Sciences Northwestern Switzerland, School of Life Sciences, Institute for Medical and Analytical Technologies, Gründenstrasse 40, 4132 Muttenz, Switzerland
[3]Biomaterials Science Center, University of Basel, Basel, Switzerland
[4]Laboratory for Surface Science and Technology, Department of Materials, ETH Zurich, Zurich, Switzerland
[5]Dipartimento di Scienze Chimiche e Geologiche, Università degli Studi di Cagliari, Cagliari, Italy

Corresponding author:
Michael de Wild, University of Applied Sciences Northwestern Switzerland, School of Life Sciences, Institute for Medical and Analytical Technologies, Gründenstrasse 40, 4132 Muttenz, Switzerland.
Email: michael.dewild@fhnw.ch

Creative Commons CC-BY-NC: This article is distributed under the terms of the Creative Commons Attribution-NonCommercial 3.0 License (http://www.creativecommons.org/licenses/by-nc/3.0/) which permits non-commercial use, reproduction and distribution of the work without further permission provided the original work is attributed as specified on the SAGE and Open Access page (http://www.uk.sagepub.com/aboutus/openaccess.htm).

to their superior mechanical properties. In particular, titanium has traditionally been one of the most commonly used metallic implant materials, demonstrating biocompatibility[5–7] and osseointegration.[8] However, the Young's modulus of Ti (100 GPa) significantly exceeds that of cortical bone (3–20 GPa), which can result in stress-shielding. As the Ti implant absorbs most of the applied mechanical load, the surrounding bone is shielded from the applied stress, ultimately leading to bone resorption.[9]

As compared to pure metals, metallic alloys allow the tuning of the particular mechanical properties toward specific medical needs (e.g., Young's modulus). In particular, nickel–titanium (NiTi) alloys have—for a metallic material—particularly low Young's moduli, which are comparable to that of bone, are pseudo-elastic, have a high damping capacity,[10] and exhibit shape memory properties. Due to this unique combination of mechanical properties, NiTi possesses great promise as a next generation scaffold material for bone repair.

To produce metallic scaffolds with a well-defined geometry, conventional methods (including turning, milling, and drilling) are often impracticable and expensive. Selective laser melting (SLM), an additive manufacturing method, is a promising alternative. Complex-shaped, porous elements or filigree lattices with strut sizes down to 200 µm can be fabricated on the basis of a predefined three-dimensional (3D) dataset.[11,12] Since pore shapes, sizes, and distributions can be controlled, specific scaffold architectures can be tailored to meet the particular needs for cell ingrowth or to match the mechanical environment of the intended implant site.[13–15] Therefore, the flexibility of the SLM technique, combined with the material properties of NiTi, allows for the design of implants with precisely tuned mechanical properties optimized for bone repair applications.

With the ultimate goal of fabricating 3D NiTi implants for spinal, orthopedic, and dental applications, in this work, we aimed to compare the behavior of human bone marrow–derived mesenchymal stromal cells (MSC) cultured on SLM-produced NiTi substrates as compared to the gold standard titanium. We first characterized the topographical and chemical surface properties of non-porous two-dimensional (2D) substrate surfaces fabricated by SLM. We next aimed to assess the proliferation and osteogenic differentiation of MSC cultured on these materials. Finally, we assessed the behavior of MSC seeded and cultured on 3D NiTi scaffolds fabricated by SLM. The cytocompatibility and osteogenic potential of SLM NiTi as demonstrated here, along with its superior mechanical properties (i.e., damping, shape memory), highlight the potential of SLM NiTi as a superior bone substitute as compared to today's Ti implant materials.

Materials and methods

SLM manufacturing of 2D disks

In order to investigate the effect of material surface properties on cell behavior, non-porous "2D" metallic disks of both nickel–titanium and titanium (∅ 14 mm, 2 mm thickness) were produced using SLM technology with the SLM Realizer 100 and Realizer 250, respectively (SLM Solutions, Lübeck, Germany). Disks were produced from either nickel–titanium with a nominal nickel-content of 55.96 wt% (Memry GmbH, Lübeck, Germany) or grade 2 titanium (SLM Solutions) with particle sizes ranging from 35 to 180 µm. Subsequent to fabrication, nickel–titanium disks were annealed for 20 min at a temperature of 500°C under a protective argon atmosphere. Disks produced by SLM were compared to disks of a conventionally manufactured reference titanium material (grade 2 Ti, non-SLM produced). Reference titanium disks were surface treated by sandblasting (abrasive grit Al_2O_3 particles with a mean grain size of 125 µm and 4 bar blasting pressure for 2 min) and acid etching (mixture of ddH_2O (resistivity 18.2 MΩcm, ELGA Purelab Option-Q DV 25, ELGA LabWater, Celle, Germany): H_2SO_4 (95%, J.T. Baker, Avantor Performance Materials, Inc., Phillipsburg, NJ, USA): HCl (32%, Sigma-Aldrich Chemie GmbH, Buchs, Switzerland) in a volume ratio of 1: 1: 2 at 93 °C for 7 min). The surface-treated reference titanium material ("Ti ref") which has been used clinically for dental implants[5,7] was provided by Thommen Medical AG (Grenchen, Switzerland).

Table 1. Sample treatment scheme. "Ti ref" is our reference material which is a conventionally manufactured and surface-treated titanium material used in the clinic.[5] A direct comparison of the effects of Ti ref and our SLM produced nickel–titanium ("NiTi") on MSC behavior is nontrivial due to a number of variables: (1) chemistry of the bulk materials, (2) the effect of the SLM manufacturing process, and (3) surface topography. Therefore, titanium disks produced by the SLM process were also fabricated ("Ti"). To account for the surface treatment of Ti ref, two groups of SLM produced disks were also surface treated ("Ti ST" and "NiTi ST") to obtain similar surface topographies..

	Ti ref	Ti	Ti ST	NiTi	NiTi ST
SLM		✓	✓	✓	✓
Sandblasting	✓		✓		
Etching	✓		✓		✓

MSC: mesenchymal stromal cells; SLM: selective laser melting.

Surface treatment of SLM disks

Considering that Ti ref disks had been surface treated, we aimed to assess the effects of surface treatment. Disks were surface treated according to the conditions outlined in Table 1. "Ti" and "NiTi" disks received no further post-processing surface treatments. Following SLM production, "Ti ST" disks were surface treated to create surfaces similar to Ti ref.[5] Ti ST disks were sandblasted and etched using similar parameters as for Ti ref. Since the titanium etching process is not effective for nickel–titanium, "NiTi ST" disks were alternatively surface treated by etching in

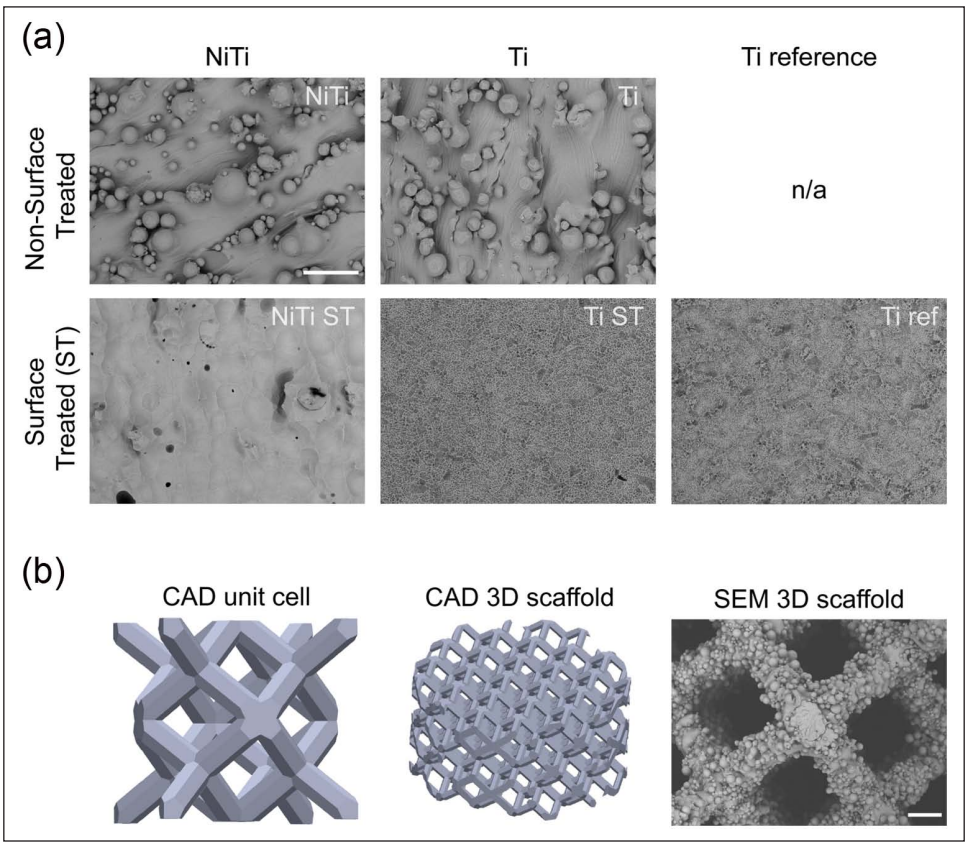

Figure 1. (a) SEM micrographs of 2D metallic disks. Upper panel depicts SLM produced NiTi and Ti disks. Lower panel depicts post-production surface treated (ST, that is, etching, passivation) disks including the clinically used reference (conventional Ti Ref). Scale bar = 100 µm and (b) CAD models of the unit cell (2 mm height), entire cylindrical 3D scaffold (4 mm height, 8 mm diameter) and SEM micrograph of the SLM produced 3D NiTi scaffold. Scale bar = 100 µm.
SEM: scanning electron microscope; 2D: two-dimensional; SLM: selective laser melting; NiTi: nickel–titanium; CAD: computer-aided design; 3D: three-dimensional.

HF at a temperature of 60°C for a duration of 3 min after SLM production.

Cleaning, passivation, and sterilization of disks

Disks were cleaned in a 4% Deconex® 15PF (Beiersdorf Münchenstein, Switzerland) solution at 90°C with ultrasonic agitation for 5 min. Specimens were then rinsed in ultrapure water (resistivity 18.2 MΩcm) for 15 min (3 × 5 min with exchange of water) in an ultrasonic bath. Subsequently, disks were passivated in nitric acid (32.5% HNO_3, Sigma-Aldrich Chemie GmbH, Buchs, Switzerland) with ultrasonic agitation for 10 min.[16] Finally, the specimens were high purity oxygen plasma treated (PDC-32G, Harrick, Ithaca, NY, USA, oxygen purity 99.9995%, Carbagas) at 29.7 W for 2 min and sterilized using hot steam (Cominox Sterilclave 24BHD, Cominox S.r.l., Carate B.za, Italia, 121°C for 20 min).

SLM manufacturing of 3D scaffolds

3D scaffolds were manufactured from nickel–titanium powder with a nominal nickel content of 55.96 wt% and particle sizes ranging between 35 and 75 µm. Smaller particles were used to fabricate 3D scaffolds compared to 2D disks to facilitate the production of small diameter filigree struts. Scaffolds were formed using a rhombic dodecahedron unit cell (height × width × depth: 2 mm × 2 mm × 2 mm, Figure 1(b)). Magics software (V15.0.4.2; Materialise, Leuven, Belgium) was used to design a scaffold with a final cylindrical shape (8 mm diameter × 4 mm height) and an overall porosity of 84%.[13] Furthermore, SLM-fabricated scaffolds exhibited a gravimetrically determined porosity of 77.5% ± 0.4% (Mettler Toledo AT261 Delta Range, Mettler-Toledo GmbH, Greifensee, Schweiz) and a porosity of 76% determined by micro-computed tomography,[17] which are slightly lower due to minimal geometric deviations during the melting process and due to residual powder particles. Following SLM production, "3D NiTi scaffolds" were post-processed as 2D NiTi disks (i.e., non-surface-treated), excluding the annealing step.

Surface characterization

Surface characterization was performed on cleaned and passivated, unsterilized samples. Surface topography was

assessed using a scanning electron microscope (SEM; FEI Nova Nano SEM 230; Microscopy Centre University Basel, Switzerland). The surface roughness was measured using 3D Confocal Laser Scanning Microscope (LEXT OLS4000; Olympus, 50× objective, Olympus Schweiz AG, Volketswil, Schweiz). Each substrate was scanned three times at random positions to determine the roughness values: average surface roughness (SR_a), maximal peak to valley height (SR_Z), and roughness spacing parameter (S_m, a measure of the mean spacing between peaks) (cutoff wavelength $\lambda_c = 51.9$ µm).[18] Additionally, the developed surface area ratio (Sdr, the ratio of the effective surface area due to the surface roughness and the projected surface area) were measured according to Wennerberg and Albrektsson.[19] Substrate wettability was evaluated by means of water contact angle measurements using a sessile drop set-up (EasyDrop; Krüss, Hamburg, Germany; MilliQ water, Millipore, MA, USA; V = 5 µL) and the corresponding software DSA 100 to calculate contact angles θ.

X-ray photoelectron spectroscopy (XPS) was carried out using a Phi Quantera SXM spectrometer (ULVAC-PHI, Chanhassen, MN, USA) equipped with a monochromatic aluminum K_α x-ray source ($h\nu$ = 1486.6 eV). Survey and high-resolution spectra were acquired from all 2D disks using a 100 µm beam diameter with the analyzer operated in fixed analyzer transmission (FAT) mode. Survey spectra were acquired setting the pass energy at 280 eV and a step size of 1.0 eV (full-width-at-half-maximum (fwhm) of the peak height for $Ag3d_{5/2}$ = 1.66 eV) while high-resolution spectra were acquired with a pass energy of 26 eV and a step size of 0.05 eV (fwhm for $Ag3d_{5/2}$ = 0.7 eV). Composition versus depth profiles were recorded alternating the etching of the sample surface with an argon source ran at 3 keV and 15 nA. The pass energy was set at 69 eV (fwhm of the peak height for $Ag3d_{5/2}$ = 0.87 eV), and the step size was 0.125 eV. Calibration of the depth scale was performed using a Si/SiO_2 reference sample under the same experimental conditions and was found to be (10.8 ± 0.1) nm/min. For data acquisition, the COMPASS software (v.7.3.4; ULVAC-PHI, Chanhassen, MN, USA) was used. Data processing and quantification of the composition depth profiles was performed using MultiPakTM 8 (V8.1C; ULVAC-PHI). Details on the spectrometer calibration are provided in Crobu et al.[20]

Cytotoxicity assessment

Cytotoxicity was assessed in accordance with ISO 10993-5.[21] Metallic substrates were immersed in complete medium (CM) consisting of alpha–minimum essential medium (MEM) supplemented with 10% fetal bovine serum (FBS), 1% HEPES, 1% sodium pyruvate, and 1% Penicillin-Streptomycin Glutamate (100×) solution (all from Gibco, Life Technologies Europe, Zug, Switzerland, http://www.invitrogen.com) with a surface to media ratio of 6 cm^2/mL for at least 24 h in a cell culture incubator. Additionally, unconditioned CM and CM conditioned with latex were used as positive and negative controls, respectively. Post extraction, metallic substrates were removed and the conditioned media used for the culture of MG-63 osteosarcoma cells. Following 3 and 7 days, the viability of MG-63 cells was determined by incubation with MTT (3-(4,5-dimethylthiazol-2-yl)-2,5-diphenyltetrazolium bromide; Sigma Aldrich) solution at a final concentration of 0.05 mg/mL. The amount of blue/purple-metabolized substrate of MTT was quantified spectroscopically by DMSO (D2650; Sigma-Aldrich Chemie GmbH, Buchs, Switzerland) extraction and absorption measurement at 575 nm wavelength (SpectraMax 190; Bucher Biotec AG, Basel, Switzerland).

Cell culture

Human bone marrow aspirates were harvested during routine iliac crest bone grafting, in accordance with the rules of the local ethical committee (University Hospital Basel, Basel, Switzerland) and after informed consent was obtained. MSC were isolated from the bone marrow aspirates[22] and expanded[23] as previously described. MSC were expanded for two to four passages for subsequent experiments.

2D cultures

For the assessment of cell proliferation, MSC were seeded onto the surfaces of metallic 2D disks and Petri dishes (i.e., tissue culture polystyrene—"TCP") at densities of 3×10^4 cells/cm^2 and cultured in CM supplemented with fibroblast growth factor–2 (FGF-2) for up to 3 weeks with media changes twice a week.

The osteogenic differentiation of MSC was performed by seeding 3×10^5 cells/cm^2 onto metallic 2D disks and 6×10^4 cells/cm^2 on TCP to reach confluence upon seeding, thereby increasing cell-to-cell contacts and accelerating the onset of osteogenic differentiation. Cells were cultured in CM or osteogenesis inducing medium (OM) consisting of CM supplemented with 10 nM dexamethasone, 0.1 mM L-ascorbic acid-2-phosphate, and 10 mM b-glycerophosphate for 2 weeks with media changes performed twice a week.

3D cultures

MSC were seeded, expanded, and differentiated within 3D NiTi scaffolds using a perfusion bioreactor system as previously described.[24,25] The bioreactor system was designed to first perfuse a cell suspension directly through the pores of a 3D scaffold, to seed cells uniformly throughout the

entire scaffold, and subsequently to perfuse culture media, to maintain cell viability during expansion and differentiation. The perfusion flow rate was set to 2.8 mL/min for 24 h during the seeding phase and subsequently changed to 0.28 mL/min for the proliferation and differentiation phases.

The proliferation of MSC on 3D NiTi scaffolds was assessed by seeding 1×10^5 cells/scaffold in the bioreactor. Cell-seeded scaffolds were subsequently cultured within the perfusion bioreactor for 3 weeks with CM supplemented with FGF-2 with media changes twice a week. To compare MSC proliferation in 3D NiTi scaffolds to proliferation on 2D disks, cells derived from one particular donor used in 2D experiments were used in the 3D scaffold experiments (n = 3 scaffold experiments).

The osteogenic differentiation capacity of MSC cultured in the 3D NiTi scaffolds was assessed by seeding 3×10^6 cells/scaffold (surface calculation based on computer-aided design (CAD) data leading to similar seeding density as on 2D metallic substrates) in the bioreactor in three independent experiments (n = 3 different donors). Cell-seeded scaffolds were subsequently cultured within the perfusion bioreactor in either OM or CM supplemented with FGF-2 for up to 3 weeks, with media changes twice a week.

Cell proliferation assay

The CyQUANT® Cell Proliferation Assay was used according to the manufacturer's protocol. Briefly, 2D disks or 3D scaffolds were washed with phosphate-buffered saline (PBS; Gibco, http://www.invitrogen.com) and frozen. Prior to the assay, a phosphate buffer–based (800 mM) enzymatic extraction protocol was carried out in order to liberate the DNA from the substrates.[26]

Imaging techniques

MSC attachment, morphology, spreading, as well as extracellular matrix (ECM) deposition were assessed using SEM (FEI Nova Nano SEM 230) following overnight cell fixation in 4% para-formaldehyde, dehydration, critical point drying, and gold sputtering.

Gene expression

Trizol® (http://www.invitrogen.com) was added to 2D disks and 3D scaffolds to extract RNA. The RNA was isolated using the NucleoSpin® RNA II kit (Macherey-Nagel, Oensingen, Switzerland, http://www.mn-net.com). RNA was eluted in RNase-free water, and transcription into complementary DNA (cDNA) was performed according to the manufacturer's protocol. The samples were analyzed using a GeneAmp® polymerase chain reaction (PCR) System 9600 (Perkin Elmer, Schwerzenbach, Switzerland, http://www.perkinelmer.com), and the transcription levels of the following genes of interest were quantified: bone sialoprotein (BSP), osteocalcin (OC),[27] and glyceraldehyde 3-phosphate dehydrogenase (GAPDH) as housekeeping gene (Primer R ATG GGG AAG GTG AAG GTC G; Primer F TAA AAG CAG CCC TGG TGA CC; Probe CGC CCA ATA CGA CCA AAT CCG TTG AC).[23]

Calcium staining

Alizarin Red (Sigma Aldrich, A5533) is an organic compound used to stain mineralized matrix in red or light purple color. After a culture period of 3 weeks, 2D disks and TCP were rinsed with PBS and fixed with formalin 4% for 10 min. After an extensive rinse with ddH_2O, 2% Alizarin Red staining solution was added to the cell layer for 10 min at room temperature. The staining solution was removed and the cell layer washed twice with pure ethanol. The samples were dried and images acquired.

Statistical analyses

For MSC cultures on metallic 2D disks, averages of four independent experiments (four different donors), with three disks per substrate and assay, were expressed as arithmetic mean ± standard deviation. For MSC cultures on 3D NiTi scaffolds, results from three independent experiments (three donors) are expressed as arithmetic mean ± standard deviation. The data were analyzed by one-way analysis of variance (ANOVA), followed by Bonferroni's post hoc test for multiple comparison (disk experiments). Differences were considered statistically significant at $p < 0.05$.

Results

Substrate characterization

SEM images in Figure 1 show the surface topographies of the metallic disks. Non-surface-treated SLM samples (NiTi and Ti) had macroscopically rough surfaces due to residues of the powder. These powder residues were sintered to the surface layer during the SLM process, and any loose particles were removed during the sonication step of the cleaning procedure. Moreover, these residues led to high arithmetic mean surface roughness values (SR_a) and to an increase in the developed surface area ratio (Sdr) (Table 2). In contrast, surface-treated samples appeared much smoother, with no powder residues remaining. The surface roughness parameters SR_a, SR_Z, Sdr, and S_m were not significantly different among the three surface-treated disks or between the two non-surface-treated disks.

Water contact angle measurements were below 90° for all disks tested (Table 2), indicating hydrophilic properties of the materials.[28] For Ti ref and NiTi, contact angle

Table 2. Measurements of contact angle (CA, static contact angle, sessile drop), arithmetic mean surface roughness (SR_a), developed surface area (Sdr), and roughness spacing parameter (S_m) of 2D metallic disks.

	Ti ref	Ti	Ti ST	NiTi	NiTi ST
CA (°)	0[a]	61 ± 8	66 ± 16	0[a]	45 ± 23
SR_a (µm)	2.1 ± 0.1	7.3 ± 1.8	3.5 ± 0.5	7.2 ± 0.6	4.3 ± 0.9
SR_Z (µm)	12.8 ± 2.7	75.0 ± 36.4	20.7 ± 15.2	65.2 ± 54.6	64.7 ± 38.9
Sdr (%)	151 ± 4	368 ± 82	201 ± 15	333 ± 55	231 ± 78
S_m	6.5 ± 2.7	12.3 ± 8.0	8.6 ± 4.9	13.8 ± 6.6	10.5 ± 5.4

2D: two-dimensional; NiTi: nickel–titanium; SD: standard deviation.
[a]No stable droplet formation. Measurements are mean ± SD (n = 3).

measurements of 0° are reported since no stable droplet formation was visible due to immediate droplet elapse, indicating extreme hydrophilicity of these materials.

Analyses of XPS survey (Figure 2(a)) and high-resolution spectra (not shown) indicate the presence of titanium oxide layers on the surface of all disks; the $Ti2p_{3/2}$ was found at 458.9 ± 0.2 eV being a typical binding energy of titanium in titanium oxide. In addition to Ti and O, NiTi ST showed Ni signals. The $Ni2p_{3/2}$ signal is multicomponent: one signal is detected at 852.4 eV and another one, with higher intensity, exhibited the peak maximum at 853.1 eV. The presence of the signal at higher binding energies indicated that the surface film after passivation contains oxidized Ni, but the layer is thin enough to allow for detection of Ni in the metallic state in the NiTi matrix.[29]

Depth profiling of the NiTi substrates showed a titanium oxide layer approximately 96 nm in thickness for NiTi and approximately 5 nm for NiTi ST (Figure 2(b)). Considering that the oxide layer is removed by surface treatment and re-formed through auto-passivation, Ti ST is expected to have an oxide layer thickness similar to NiTi ST. In this work, the oxide layer thickness is estimated to be higher than 6.5 nm using the inelastic mean free path of the signal of titanium oxide (TiO) at 455.1 eV. Surface-treated titanium implants have been shown to exhibit oxide layer thicknesses in the range of 1.5 to 10 nm,[30] consistent with the native oxide layer previously measured on Ti ref.[31] Carbon and sodium were only detected in the outermost layer due to the exposure to the ambient atmosphere. These signals disappeared after the first Ar^+ sputtering cycle.

Cytotoxicity assessment

Assessment of the viability of MG-63 cells via MTT staining revealed no cytotoxic effect of NiTi and NiTi ST according to ISO 10993-5. MG-63 metabolic activity on NiTi and NiTi ST were determined to be 1.01 ± 0.10-fold and 0.98 ± 0.10-fold as compared to positive controls; latex negative control was 0.16 ± 0.01-fold compared to positive controls.

2D culture

Proliferation assessment. Proliferation studies were carried out with four independent donors. No significant differences in the growth rate of MSC could be observed for any of the materials as compared to Ti ref or among any of the materials (Figure 3).

Cell morphology. SEM images were acquired after 11 days (depicting an intermediate time point of differentiation; data not shown) of MSC culture on metallic disks in CM and OM. Cell morphology was similar for all metallic substrates. However, morphological differences were observed between MSC cultured in CM as compared to OM. MSC cultured in CM had a randomly oriented, branched, and flat morphology, whereas MSC cultured in OM aligned themselves and branched only into a preferred axis. Interestingly, cells cultured on non-surface-treated disks had adhered to both the underlying substratum as well as the powder residues.

To investigate ECM production by differentiated MSC, SEM images were acquired after 21 days (Figure 4(a)). On all disks, dense cell layers with high amounts of ECM were observed. MSC cultured on surface-treated disks (NiTi ST, Ti ST, and Ti ref) exhibited a spindle-like shape with random orientation in CM and an aligned orientation in OM. MSC cultured on non-surface-treated disks (Ti and NiTi) were almost indistinguishable from the abundant ECM, hindering the assessment of their morphology.

Osteogenic differentiation. BSP gene expression levels were similar for MSC cultured on all materials ($p > 0.5$ for CM and $p > 0.08$ for OM) (Figure 4(b)). However, expression of OC was down-regulated for MSC cultured in OM on NiTi (3-fold; $p < 0.05$) and NiTi ST (6-fold; $p < 0.05$) as compared to Ti ref. For all materials, BSP expression was significantly higher when MSC were cultured in OM as compared to CM on the respective materials ($p < 0.001$).

Alizarin Red staining of CM cultured MSC showed similar faint staining for all materials tested. In contrast, with the exception of TCP, high matrix mineralization was observed when MSC were cultured in OM on all of the metallic disks (Figure 4(c)).

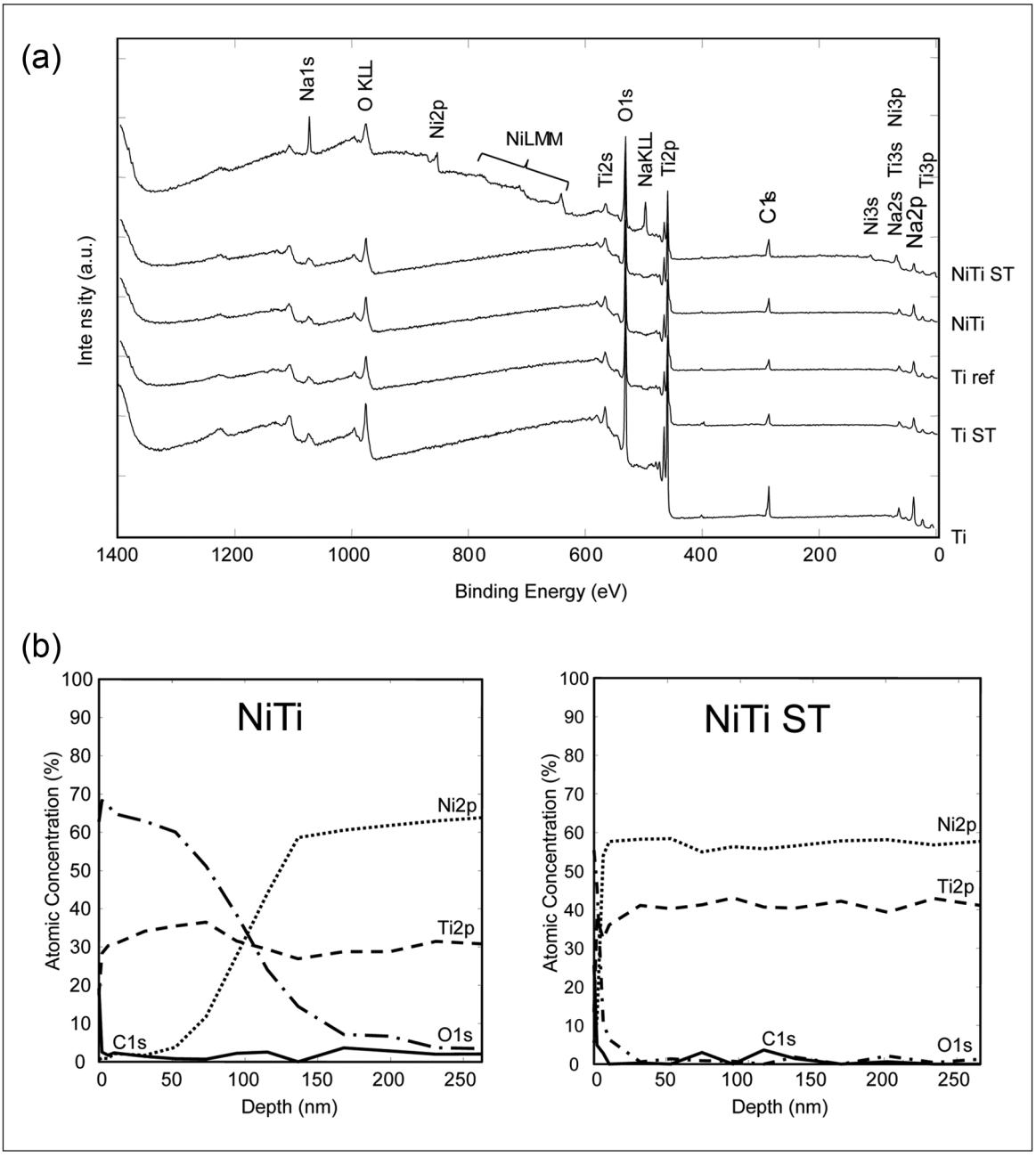

Figure 2. (a) XPS survey spectra of 2D disks indicated the presence of a titanium oxide layer on the surface of the materials. Ni could be detected on the surface of NiTi ST. (b) XPS depth profile for NiTi and NiTi ST revealed oxide layer thicknesses of approximately 96 nm and 5 nm, respectively. Approximate depths were estimated according to the sputter rate on Si/SiO_2 reference sample (10.8 ± 0.1 nm/min).
XPS: x-ray photoelectron spectroscopy; 2D: two-dimensional; NiTi: nickel–titanium.

3D culture

Proliferation and cell morphology assessment. MSC proliferated at similar rates, independent of whether the cells were cultured on porous 3D scaffolds or on 2D disks of SLM NiTi (3D: 0.28 ± 0.04 doublings/day; 2D: 0.32 ± 0.02 doublings/day).

Following 14 days of 3D culture, MSC cultured in CM had colonized the entire scaffold, being homogeneously distributed along the struts of the scaffold at the periphery as well as the struts throughout the internal region (Figure 5(a), upper panel). However, the pore volume remained relatively empty within CM cultured constructs. In contrast, MSC cultured in OM were not only homogeneously distributed along the scaffold struts but were also embedded within ECM filling the volume of the scaffold pores (Figure 5(a), lower panel).

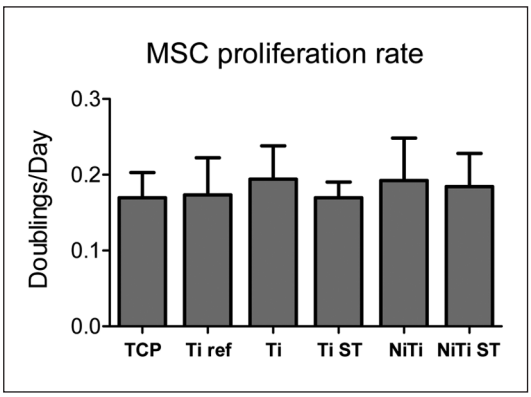

Figure 3. Proliferation rate (doublings/day) of MSC cultured on 2D disks for 1 week.
TCP: tissue culture polystyrene; NiTi: nickel–titanium; MSC: mesenchymal stromal cells; 2D: two-dimensional; SD: standard deviation.
No significance differences were observed between the substrates tested. Measurements are mean ± SD (n = 4).

Osteogenic differentiation. BSP gene expression levels were significantly up-regulated when MSC were cultured on 3D NiTi for either 2 or 3 weeks in OM as compared to CM (Figure 5(b)). In contrast to results for 2D cultures, expression of OC was significantly up-regulated when MSC were cultured on 3D NiTi scaffolds in OM as compared to CM. Expression of both BSP and OC was significantly higher when MSC were cultured in osteogenic medium on the 3D NiTi scaffolds as compared to 2D NiTi disks ($p < 0.01$).

Discussion

In this work, we have demonstrated that the proliferation and osteogenic differentiation capacity of human MSC is similar when cultured on SLM NiTi as compared to a clinically used titanium implant material. We have further shown that when cultured in SLM-produced, porous 3D NiTi scaffolds, MSC colonized the scaffolds, differentiated osteogenically, and filled the pore volume with extracellular matrix.

The surface roughness has been demonstrated to affect cell behavior;[32–35] therefore, we quantitatively and qualitatively assessed the surface topography of the 2D disks. Materials with a higher surface roughness have been demonstrated to favor cell attachment due to enhanced protein binding to the surface,[32] and to increase osteogenic differentiation[33,34] but impair cell proliferation.[33,35] In our study, while non-surface-treated NiTi and Ti had significantly higher values of SR_a than Ti ref, the differences in roughness did not affect MSC proliferation or osteogenic differentiation. It has been demonstrated that bone response was influenced by the implant surface topography at the micro- and nanometer scales. Based on the extent of osseointegration, surface roughness was thus categorized as (1) smooth ($SR_a < 0.5$ μm), (2) minimally rough (SR_a 0.5–1 μm), (3) moderately rough ($SR_a > 1$–2 μm), and (4) rough ($SR_a > 2$ μm) surfaces.[36,37] Moderately rough and rough surfaces showed the strongest bone response in terms of osseointegration. In our study, all 2D disks, whether surface treated or not, would be classified as "rough," since values of SR_a were larger than 2 μm, possibly explaining the similar response of MSC among the groups.

The surfaces of all disks fabricated in this study were found to have contact angles of $\theta < 90$ °, defining them as hydrophilic.[38] It was previously shown that MSC gene expression of osteogenic markers was generally higher on hydrophilic as compared to hydrophobic surfaces, however at the expense of impaired cell adhesion and proliferation.[38,39] In our study, MSC not only showed signs of osteogenic differentiation but extensively proliferated on all substrates as well.

Although nickel is known to exhibit cytotoxic effects[40] as an intermetallic component of the NiTi alloy, it has been demonstrated to be biocompatible.[41,42] Our study is consistent with others,[43] showing that the SLM processing of NiTi does not impair its cytocompatibility. Moreover, SLM processed NiTi has been demonstrated to be biocompatible.[44] The cytocompatibility and biocompatibility of NiTi arise from auto-passivation,[45] which creates an inert titanium oxide surface layer (Figure 2(b)) that prevents the release of Ni^{2+}.[46] An oxide layer 1.5–10 nm in thickness is also spontaneously formed on Ti substrates when in contact with oxygen.[30] The XPS data shown in Figure 2 confirm the presence of oxide layers on all of our NiTi and Ti disks. Surface oxides are known to spontaneously nucleate calcium phosphate (apatite) when in contact with physiological fluids.[47,48] The nucleated apatite (hydroxyapatite) triggers cell attachment as well as cell differentiation.[49,50] Larsson et al.[51] demonstrated that implants with an oxide layer improved the degree of bone contact area and bone formation. Moreover, the thickness of the oxide layer can also play a crucial role. Electropolished Ti, with a depleted oxide layer of only 2–3 nm in thickness, was associated with decreased bone formation around the implant as compared to auto-passivated Ti.[51] On the other hand, Sul et al.[52] showed that Ti, which was thermally treated to increase the thickness of the oxide layer to 200 and 1000 nm, had significantly stronger bone response with the thickest oxide layer. However, no significant differences were reported for oxide layers generated by auto-passivation and oxide layers up to 200 nm.[52] Therefore, our work appears consistent with Sul et al.,[52] since MSC had similar responses on all disks, which exhibited native oxide layers with thicknesses (ranging from 5–96 nm) below the threshold of 200 nm.

NiTi and Ti substrates incorporated residual metallic powder particles onto their surface, which increased the overall roughness and led to relatively high micrometer-scale peaks. As seen by SEM, these peaks appeared to serve as additional attachment points for cells, possibly imposing pseudo-3D properties to cells, leading to multiple cell layers with increased cell-to-cell and cell-to-ECM contacts. In contrast, cells cultured on the smoother

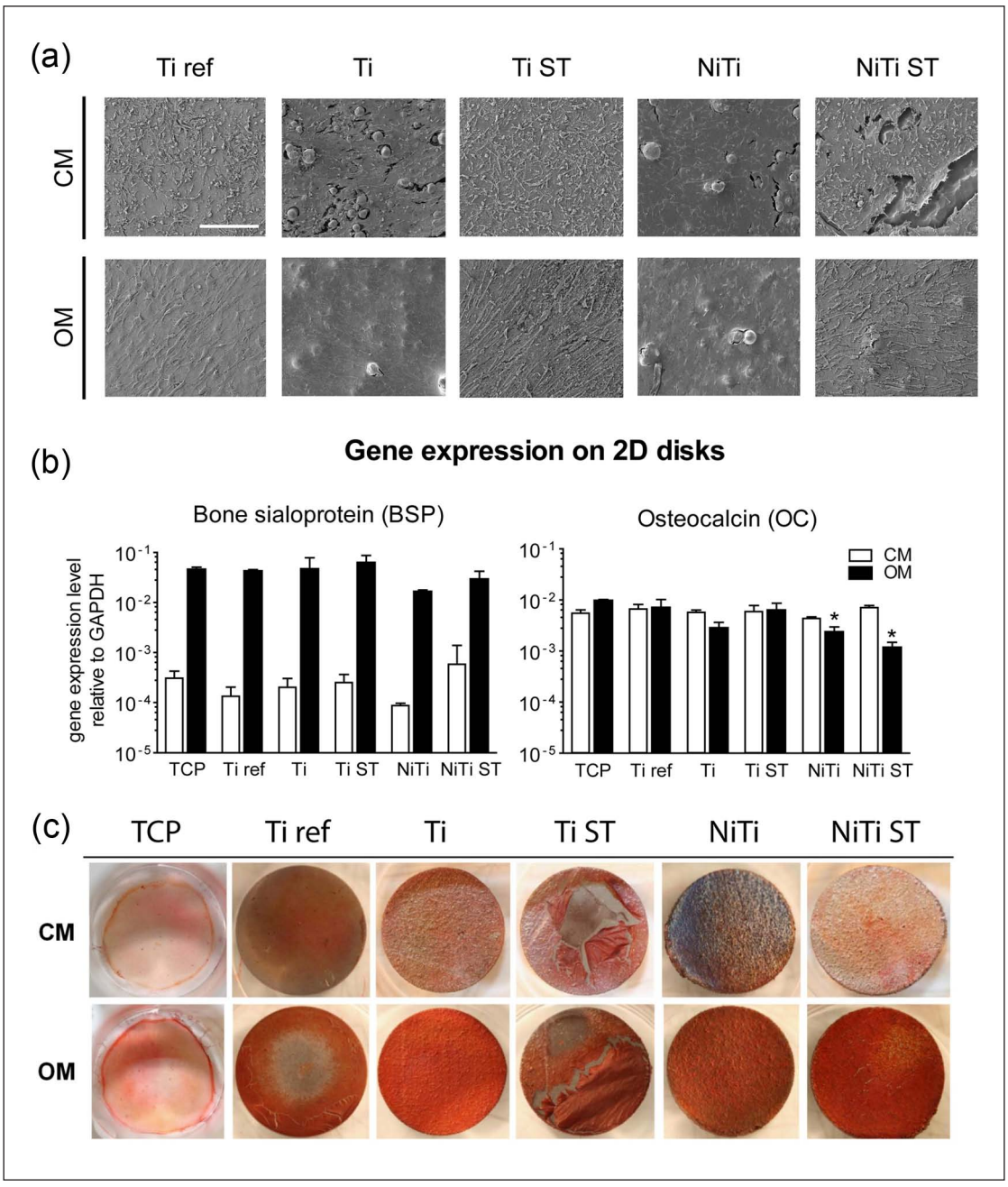

Figure 4. (a) SEM micrographs of MSC cultured on 2D metallic disks for 21 days. MSC colonized the entire substrate surfaces and produced high amounts of extracellular matrix (ECM). Scale bar = 200 µm. (b) Gene expression levels for MSC cultured on 2D disks for 14 days. BSP was up-regulated for MSC cultured in OM. Levels of OC were slightly down-regulated for MSC cultured in OM on Ti, NiTi, and NiTi ST. Measurements are mean ± SD (n = 3).*p<0.05, **p<0.01, as compared to Ti ref in corresponding medium. (c) Alizarin Red Staining of 2D disks following 2 weeks of MSC culture depicting matrix mineralization for MSC cultured in OM on metallic disks.

CM: complete medium; OM: osteogenesis inducing medium; SEM: scanning electron microscope; MSC: mesenchymal stromal cells; 2D: two-dimensional; NiTi: nickel–titanium; SD: standard deviation.

surface-treated samples did not build-up multi-layered colonies as observed with the non-surface-treated samples. Nevertheless, the results show similar proliferation rates and differentiation capacities on surface-treated and non-surface-treated disks, indicating a negligible effect of the residual powder particles.

BSP correlates with the initial phase of matrix mineralization and was proposed to be the main nucleator of hydroxyapatite crystals.[53] OC is the most abundant non-collagenous bone-matrix protein,[54,55] which is synthesized by osteoblasts in the late differentiation state[56] and induced at the onset of extracellular matrix mineralization.[57] High

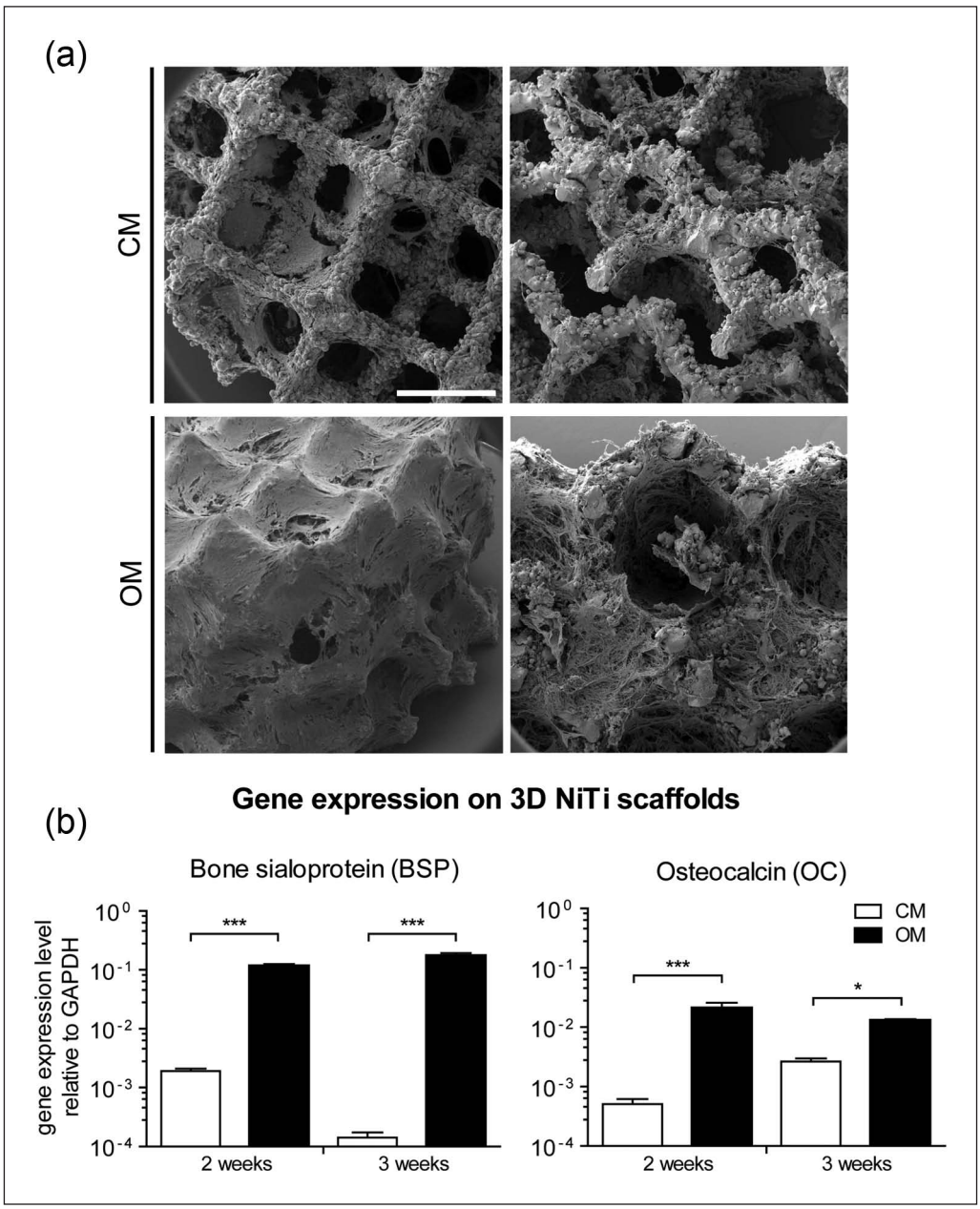

Figure 5. (a) SEM micrographs of cells cultured on 3D NiTi scaffolds in CM or OM, for 14 days. Left panels depict view on the periphery of the scaffolds. Right panels depict the scaffold interior. Scale bar = 1 mm. High amounts of ECM were observed for OM-cultured MSC. (b) Gene expression levels of MSC cultured on 3D NiTi scaffolds for 2 weeks and 3 weeks. Both BSP and OC were up-regulated when MSC were cultured in OM.
SEM: scanning electron microscope; 3D: three-dimensional; NiTi: nickel–titanium; CM: complete medium; OM: osteogenesis inducing medium; ECM: extracellular matrix; MSC: mesenchymal stromal cells; SD: standard deviation.
Measurements are mean ± SD (n = 3).
*$p < 0.05$, ***$p < 0.001$.

expression levels of both BSP and OC on each of the materials tested highlight a similar capacity of MSC to differentiate along the osteogenic lineage when cultured on NiTi as on the conventional Ti ref. Moreover, Alizarin red staining underlines similar levels of matrix mineralization by MSC on NiTi as compared to Ti ref (Figure 4(c)).

After demonstrating that SLM NiTi can support the osteogenic differentiation and matrix mineralization of MSC in our 2D disk model system, we next aimed to investigate the effect of a 3D environment of a SLM NiTi scaffold. Design of the scaffold architecture was based on criteria supporting vascularization and integration of an implant,[58] as well as

finite element modeling of stress/strain profiles within the scaffold under compressive loading.[13] First, we determined that growth rates of MSC cultured in 3D NiTi scaffolds were similar to growth rates on 2D disks. As seen by SEM (Figure 5(a)), MSC colonized the 3D scaffold struts and, when osteogenically induced, filled the porous volume of the scaffold with extracellular matrix. Similar to the 2D disk model system, both BSP and OC were also highly expressed by MSC cultured in the 3D NiTi scaffolds in osteogenic medium. Interestingly, expression of both BSP and OC was significantly higher when MSC were osteogenically differentiated within the 3D environment of the NiTi scaffolds as compared to on the 2D surface of NiTi disks. This is consistent with other studies, which have shown that more osteoinductive constructs could be generated by culturing MSC in a 3D scaffold as compared to culturing MSC in 2D.[22,59] Taken together, the high proliferation rate, differentiation capacity, and high ECM production of MSC on 3D NiTi scaffolds highlight the potential of NiTi as a scaffold for bone tissue engineering applications.

Considering the adhesion, proliferation, and differentiation capacity of MSC on SLM NiTi, this study also presents the possibility to utilize 3D NiTi scaffolds as a cell-free implant material for bone repair. In vivo, small numbers of MSC from the blood or bone marrow in the repair site could infiltrate the scaffolds, adhere to their surface, and proliferate. This could result in the colonization of the scaffold, subsequent differentiation of MSC down the osteogenic linage, and ultimately lead to accelerated osseointegration of the implant.

In addition, porous NiTi scaffolds that are able to switch between defined structural states (shape memory), induced either mechanically or thermally,[13] represent a further approach to study the response of cells and tissues to physiological strains in vitro.[60,61] For example, Strauß et al.[62] determined that static compression of NiTi scaffolds was able to trigger osteogenic differentiation of adipose tissue–derived stem cells. Further investigations might lead to implants that apply physiological strains via shape memory properties that trigger cell differentiation and bone tissue ingrowth. These advanced implants might actively stimulate the surrounding tissue through the application of micro-motions leading to profound reductions in implant integration periods and ultimately to faster patient recoveries.

Conclusion

We have demonstrated that MSC cultured on rapid-prototyped NiTi proliferated and differentiated along the osteogenic lineage to similar extents as on the clinically used reference titanium material. These results highlight the potential of SLM NiTi as a scaffold material for bone tissue engineering applications (i.e., in vitro engineering of osteogenic grafts) as well as regenerative medicine approaches (i.e., as a cell-free implant material). Moreover, the flexibility of the SLM technique, combined with the unique mechanical properties of NiTi, would allow for the design of grafts/implants better matching the mechanical requirements of a bone repair site than conventional Ti implants. Finally, the development of advanced NiTi shape memory implants, capable of applying regenerative mechanical stimuli at the site of implantation, could have profound consequences on implant integration periods leading to faster patient recoveries[63] and to more successful clinical outcomes in the long term.

Acknowledgements

The authors thank Matthias Mertmann and Ulrich Mürrle from Memry GmbH, Weil am Rhein, Germany for the supply of pre-alloyed nickel–titanium (NiTi) powders and the surface treatment of selective laser melting (SLM) NiTi specimens and Falko Schlottig from Thommen Medical AG, Grenchen, Switzerland for the kind supply of titanium reference samples. Furthermore, we thank Daniel Mathys, scanning electron microscope (SEM) specialist at the Microscopy Center of the University of Basel; Nicholas D. Spencer for his kind hospitality; and Giovanni Cossu, technical engineer at LSST–ETH Zurich, for his help during the x-ray photoelectron spectroscopy (XPS) measurements. We also appreciate the critical review of the project by Marcus Textor.

Declaration of conflicting interests

The authors declare that there is no conflict of interest.

Funding

The authors gratefully acknowledge the funding of the Swiss National Science Foundation within the research program NRP 62 "Smart Materials" (Grant No. 406240_126123).

References

1. Hutmacher DW, Schantz JT, Lam CXF, et al. State of the art and future directions of scaffold-based bone engineering from a biomaterials perspective. *J Tissue Eng Regen Med* 2007; 1(4): 245–260, http://dx.doi.org/10.1002/term.24
2. Salgado AJ, Coutinho OP and Reis RL. Bone tissue engineering: state of the art and future trends. *Macromol Biosci* 2004; 4(8): 743–765, http://dx.doi.org/10.1002/mabi.200400026
3. Rezwan K, Chen QZ, Blaker JJ, et al. Biodegradable and bioactive porous polymer/inorganic composite scaffolds for bone tissue engineering. *Biomaterials* 2006; 27(18): 3413–3431, http://www.sciencedirect.com/science/article/pii/S0142961206001232
4. Albrektsson T and Johansson C. Osteoinduction, osteoconduction and osseointegration. *Eur Spine J* 2001; 10(Suppl. 2): S96–S101, http://link.springer.com/article/10.1007/s005860100282 (accessed 6 November 2013).
5. Tugulu S, Lowe K, Scharnweber D, et al. Preparation of superhydrophilic microrough titanium implant surfaces by

alkali treatment. *J Mater Sci Mater Med* 2010; 21(10): 2751–2763, http://www.ncbi.nlm.nih.gov/pubmed/20725770
6. Germanier Y, Tosatti S, Broggini N, et al. Enhanced bone apposition around biofunctionalized sandblasted and acid-etched titanium implant surfaces. A histomorphometric study in miniature pigs. *Clin Oral Implants Res* 2006; 17(3): 251–257, http://www.ncbi.nlm.nih.gov/pubmed/16672019 (accessed 12 November 2012).
7. Milleret V, Tugulu S, Schlottig F, et al. Alkali treatment of microrough titanium surfaces affects macrophage/monocyte adhesion, platelet activation and architecture of blood clot formation. *Eur Cell Mater* 2011; 21: 430–444, http://www.ncbi.nlm.nih.gov/pubmed/21604243
8. Nag S and Banerjee R. Fundamentals of medical implant materials. In: Narayan R (ed.) *ASM handbook, volume 23: materials for medical devices*. Materials Park, OH: ASM International, 2012, pp. 6–17.
9. Huiskes R, Weinans H and van Rietbergen B. The relationship between stress shielding and bone resorption around total hip stems and the effects of flexible materials. *Clin Orthop Relat Res* 1992; 274: 124–134, http://www.ncbi.nlm.nih.gov/pubmed/1728998 (accessed 19 August 2013).
10. De Wild M, Meier F, Bormann T, et al. Damping of selective-laser-melted NiTi for medical implants. *J Mater Eng Perform* 2014, http://link.springer.com/10.1007/s11665-014-0889-8 (accessed 17 February 2014).
11. Mullen L, Stamp RC, Brooks WK, et al. Selective Laser Melting: a regular unit cell approach for the manufacture of porous, titanium, bone in-growth constructs, suitable for orthopedic applications. *J Biomed Mater Res B Appl Biomater* 2009; 89(2): 325–334, http://www.ncbi.nlm.nih.gov/pubmed/18837456 (accessed 28 February 2014).
12. Pattanayak DK, Fukuda A, Matsushita T, et al. Bioactive Ti metal analogous to human cancellous bone: fabrication by selective laser melting and chemical treatments. *Acta Biomater* 2011, http://www.sciencedirect.com/science/article/B7GHW-51491KH-C/2/408b9a0545d42b82221a0f73be480024
13. Bormann T, Schulz G, Deyhle H, et al. Combining micro computed tomography and three-dimensional registration to evaluate local strains in shape memory scaffolds. *Acta Biomater* 2013; 10(2): 1024–1034, http://www.ncbi.nlm.nih.gov/pubmed/24257506 (accessed 22 November 2013).
14. Sobral JM, Caridade SG, Sousa RA, et al. Three-dimensional plotted scaffolds with controlled pore size gradients: effect of scaffold geometry on mechanical performance and cell seeding efficiency. *Acta Biomater* 2011; 7(3): 1009–1018, http://www.ncbi.nlm.nih.gov/pubmed/21056125 (accessed 14 March 2014).
15. Van Bael S, Chai YC, Truscello S, et al. The effect of pore geometry on the in vitro biological behavior of human periosteum-derived cells seeded on selective laser-melted Ti6Al4V bone scaffolds. *Acta Biomater* 2012; 8(7): 2824–2834, http://www.ncbi.nlm.nih.gov/pubmed/22487930 (accessed 18 February 2014).
16. Zhao G, Zinger O, Schwartz Z, et al. Osteoblast-like cells are sensitive to submicron-scale surface structure. *Clin Oral Implants Res* 2006; 17(3): 258–264, http://www.ncbi.nlm.nih.gov/pubmed/16672020 (accessed 19 August 2013).
17. Bormann T, de Wild M, Beckmann F, et al. Assessing the morphology of selective laser melted NiTi-scaffolds for a three-dimensional quantification of the one-way shape memory effect. In: (ed NC Goulbourne and HE Naguib), 2013, p. 868914, http://proceedings.spiedigitallibrary.org/proceeding.aspx?doi=10.1117/12.2012245 (accessed 20 May 2014).
18. Olympus. *User's manual: confocal scanning laser microscope LEXT OLS3100*. Hamburg: Olympus Life Science Europa GMBH, 2008.
19. Wennerberg A and Albrektsson T. On implant surfaces: a review of current knowledge and opinions. *Int J Oral Maxillofac Implants* 2009; 25(1): 63–74, http://www.ncbi.nlm.nih.gov/pubmed/20209188
20. Crobu M, Rossi A, Mangolini F, et al. Chain-length-identification strategy in zinc polyphosphate glasses by means of XPS and ToF-SIMS. *Anal Bioanal Chem* 2012; 403(5): 1415–1432, http://www.ncbi.nlm.nih.gov/pubmed/22451170 (accessed 2 April 2014).
21. ISO 10993-5:2009. Biological evaluation of medical devices—part 5: tests for in vitro cytotoxicity.
22. Braccini A, Wendt D, Jaquiery C, et al. Three-dimensional perfusion culture of human bone marrow cells and generation of osteoinductive grafts. *Stem Cells* 2005; 23(8): 1066–1072, http://www.ncbi.nlm.nih.gov/pubmed/16002780 (accessed 12 August 2013).
23. Frank O, Heim M, Jakob M, et al. Real-time quantitative RT-PCR analysis of human bone marrow stromal cells during osteogenic differentiation in vitro. *J Cell Biochem* 2002; 85(4): 737–746, http://www.ncbi.nlm.nih.gov/pubmed/11968014
24. Wendt D, Marsano A, Jakob M, et al. Oscillating perfusion of cell suspensions through three-dimensional scaffolds enhances cell seeding efficiency and uniformity. *Biotechnol Bioeng* 2003; 84(2): 205–214, http://www.ncbi.nlm.nih.gov/pubmed/12966577
25. Wendt D, Stroebel S, Jakob M, et al. Uniform tissues engineered by seeding and culturing cells in 3D scaffolds under perfusion at defined oxygen tensions. *Biorheology* 2006; 43(3–4): 481–488, http://www.ncbi.nlm.nih.gov/pubmed/16912419
26. Piccinini E, Sadr N and Martin I. Ceramic materials lead to underestimated DNA quantifications: a method for reliable measurements. *Eur Cell Mater* 2010; 20: 38–44, http://www.ncbi.nlm.nih.gov/pubmed/20652860 (accessed 22 November 2012).
27. Barbero A, Ploegert S, Heberer M, et al. Plasticity of clonal populations of dedifferentiated adult human articular chondrocytes. *Arthritis Rheum* 2003; 48(5): 1315–1325, http://www.ncbi.nlm.nih.gov/pubmed/12746904
28. Vogler EA. Structure and reactivity of water at biomaterial surfaces. *Adv Colloid Interface Sci* 1998; 74: 69–117, http://www.ncbi.nlm.nih.gov/pubmed/9561719 (accessed 12 November 2012).
29. Addari D, Mignani A, Scavetta E, et al. An XPS investigation on glucose oxidase and Ni/Al hydrotalcite interaction. *Surf Interface Anal* 2011; 43(4): 816–822, http://doi.wiley.com/10.1002/sia.3636 (accessed 2 April 2014).
30. Sul YT, Johansson CB, Jeong Y, et al. Oxidized implants and their influence on the bone response. *J Mater Sci Mater Med* 2001; 12(10–12): 1025–1031, http://www.ncbi.nlm.nih.gov/pubmed/15348359 (accessed 4 March 2014).

31. Kang B-S, Sul Y-T, Oh S-J, et al. XPS, AES and SEM analysis of recent dental implants. *Acta Biomater* 2009; 5(6): 2222–2229, http://www.ncbi.nlm.nih.gov/pubmed/19261554 (accessed 4 March 2014).
32. Deligianni DD, Katsala N, Ladas S, et al. Effect of surface roughness of the titanium alloy Ti-6Al-4V on human bone marrow cell response and on protein adsorption. *Biomaterials* 2001; 22(11): 1241–1251, http://www.ncbi.nlm.nih.gov/pubmed/11336296 (accessed 26 February 2014).
33. Hempel U, Hefti T, Dieter P, et al. Response of human bone marrow stromal cells, MG-63, and SaOS-2 to titanium-based dental implant surfaces with different topography and surface energy. *Clin Oral Implants Res* 2013; 24(2): 174–82, http://dx.doi.org/10.1111/j.1600-0501.2011.02328.x (accessed 12 May 2014).
34. Martin JY, Schwartz Z, Hummert TW, et al. Effect of titanium surface roughness on proliferation, differentiation, and protein synthesis of human osteoblast-like cells (MG63). *J Biomed Mater Res* 1995; 29(3): 389–401, http://www.ncbi.nlm.nih.gov/pubmed/7542245 (accessed 4 February 2013).
35. Ponsonnet L, Comte V, Othmane A, et al. Effect of surface topography and chemistry on adhesion, orientation and growth of fibroblasts on nickel–titanium substrates. *Mater Sci Eng C* 2002; 21(1–2): 157–165, http://linkinghub.elsevier.com/retrieve/pii/S0928493102000978 (accessed 4 February 2013).
36. Wennerberg A and Albrektsson T. Effects of titanium surface topography on bone integration: a systematic review. *Clin Oral Implants Res* 2009; 20(Suppl. 4): 172–184, http://www.ncbi.nlm.nih.gov/pubmed/19663964 (accessed 28 November 2013).
37. Rønold HJ, Lyngstadaas SP and Ellingsen JE. Analysing the optimal value for titanium implant roughness in bone attachment using a tensile test. *Biomaterials* 2003; 24(25): 4559–4564, http://linkinghub.elsevier.com/retrieve/pii/S0142961203002564 (accessed 4 December 2013).
38. Rupp F, Scheideler L, Olshanska N, et al. Enhancing surface free energy and hydrophilicity through chemical modification of microstructured titanium implant surfaces. *J Biomed Mater Res A* 2006; 76(2): 323–334, http://www.ncbi.nlm.nih.gov/pubmed/16270344 (accessed 23 May 2013).
39. Mamalis AA and Silvestros SS. Analysis of osteoblastic gene expression in the early human mesenchymal cell response to a chemically modified implant surface: an in vitro study. *Clin Oral Implants Res* 2011; 22(5): 530–537, http://www.ncbi.nlm.nih.gov/pubmed/21121959 (accessed 23 May 2013).
40. Putters JLM, Kaulesar Sukul DMKS, de Zeeuw GR, et al. Comparative cell culture effects of shape memory metal (Nitinol®), nickel and titanium: a biocompatibility estimation. *Eur Surg Res* 1992; 24(6): 378–382, http://www.karger.com/DOI/10.1159/000129231
41. Habijan T, Bremm O, Esenwein SA, et al. Influence of nickel ions on human multipotent mesenchymal stromal cells (hMSCs). *Materwiss Werksttech* 2007; 38(12): 969–974, http://doi.wiley.com/10.1002/mawe.200700231 (accessed 12 November 2012).
42. Es-Souni MM and Fischer-Brandies H. Assessing the biocompatibility of NiTi shape memory alloys used for medical applications. *Anal Bioanal Chem* 2005; 381(3): 557–567, http://www.ncbi.nlm.nih.gov/pubmed/15660223 (accessed 12 February 2013).
43. Habijan T, Haberland C, Meier H, et al. The biocompatibility of dense and porous Nickel–Titanium produced by selective laser melting. *Mater Sci Eng C* 2013; 33(1): 419–426, http://linkinghub.elsevier.com/retrieve/pii/S0928493112004407 (accessed 13 November 2012).
44. Shishkovsky IV, Volova LT, Kuznetsov MV, et al. Porous biocompatible implants and tissue scaffolds synthesized by selective laser sintering from Ti and NiTi. *J Mater Chem* 2008; 18(12): 1309–1317, http://xlink.rsc.org/?DOI=b715313a (accessed 30 April 2014).
45. Chan C-M, Trigwell S and Duerig T. Oxidation of an NiTi alloy. *Surf Interface Anal* 1990; 15(6): 349–354, http://dx.doi.org/10.1002/sia.740150602 (accessed 19 May 2014).
46. Shabalovskaya SA, Tian H, Anderegg JW, et al. The influence of surface oxides on the distribution and release of nickel from Nitinol wires. *Biomaterials* 2009; 30(4): 468–477, http://dx.doi.org/10.1016/j.biomaterials.2008.10.014 (accessed 18 February 2013).
47. Li P, Ohtsuki C, Kokubo T, et al. The role of hydrated silica, titania, and alumina in inducing apatite on implants. *J Biomed Mater Res* 1994; 28(1): 7–15, http://dx.doi.org/10.1002/jbm.820280103 (accessed 4 March 2014).
48. Sundgren JE, Bodö P, Lundström I, et al. Auger electron spectroscopic studies of stainless-steel implants. *J Biomed Mater Res* 1985; 19(6): 663–671, http://dx.doi.org/10.1002/jbm.820190606 (accessed 4 March 2014).
49. Habibovic P, Sees TM, van den Doel MA, et al. Osteoinduction by biomaterials—physicochemical and structural influences. *J Biomed Mater Res Part A* 2006; 77(4): 747–762, http://dx.doi.org/10.1002/jbm.a.30712
50. Yoshikawa H and Myoui A. Bone tissue engineering with porous hydroxyapatite ceramics. *J Artif Organs* 2005; 8(3): 131–136, http://www.ncbi.nlm.nih.gov/pubmed/16235028 (accessed 4 March 2014).
51. Larsson C, Thomsen P, Aronsson BO, et al. Bone response to surface-modified titanium implants: studies on the early tissue response to machined and electropolished implants with different oxide thicknesses. *Biomaterials* 1996; 17(6): 605–616, http://www.ncbi.nlm.nih.gov/pubmed/8652779 (accessed 4 March 2014).
52. Sul Y-T, Johansson CB, Jeong Y, et al. Resonance frequency and removal torque analysis of implants with turned and anodized surface oxides. *Clin Oral Implants Res* 2002; 13(3): 252–259, http://www.ncbi.nlm.nih.gov/pubmed/12010155 (accessed 4 March 2014).
53. Bianco P, Riminucci M, Silvestrini G, et al. Localization of bone sialoprotein (BSP) to Golgi and post-Golgi secretory structures in osteoblasts and to discrete sites in early bone matrix. *J Histochem Cytochem* 1993; 41(2): 193–203, http://www.ncbi.nlm.nih.gov/pubmed/8419459 (accessed 12 March 2013).
54. Wolf G. Function of the bone protein osteocalcin: definitive evidence. *Nutr Rev* 1996; 54(10): 332–323, http://doi.wiley.com/10.1111/j.1753-4887.1996.tb03798.x (accessed 12 March 2013).
55. Hauschka PV, Lian JB, Cole DE, et al. Osteocalcin and matrix Gla protein: vitamin K-dependent proteins in bone. *Physiol Rev* 1989; 69(3): 990–1047, http://www.ncbi.nlm.nih.gov/pubmed/2664828 (accessed 28 August 2013).

56. Neve A, Corrado A and Cantatore FP. Osteocalcin: skeletal and extra-skeletal effects. *J Cell Physiol* 2013; 228(6): 1149–1153, http://dx.doi.org/10.1002/jcp.24278
57. Lian JB and Stein GS. Concepts of osteoblast growth and differentiation: basis for modulation of bone cell development and tissue formation. *Crit Rev Oral Biol Med* 1992; 3: 269–305.
58. Hollister SJ. Porous scaffold design for tissue engineering. *Nat Mater* 2005; 4(7): 518–524, http://www.ncbi.nlm.nih.gov/pubmed/16003400 (accessed 12 November 2012).
59. Scherberich A, Galli R, Jaquiery C, et al. Three-dimensional perfusion culture of human adipose tissue-derived endothelial and osteoblastic progenitors generates osteogenic constructs with intrinsic vascularization capacity. *Stem Cells* 2007; 25(7): 1823–1829, http://www.ncbi.nlm.nih.gov/pubmed/17446558 (accessed 20 March 2014).
60. Byrne EM, Farrell E, McMahon LA, et al. Gene expression by marrow stromal cells in a porous collagen-glycosaminoglycan scaffold is affected by pore size and mechanical stimulation. *J Mater Sci Mater Med* 2008; 19(11): 3455–3463, http://www.ncbi.nlm.nih.gov/pubmed/18584120 (accessed 31 January 2013).
61. Van Eijk F, Saris DBF, Creemers LB, et al. The effect of timing of mechanical stimulation on proliferation and differentiation of goat bone marrow stem cells cultured on braided PLGA scaffolds. *Tissue Eng Part A* 2008; 14(8): 1425–1433, http://www.ncbi.nlm.nih.gov/pubmed/18637726 (accessed 30 January 2013).
62. Strauß S, Dudziak S, Hagemann R, et al. Induction of osteogenic differentiation of adipose derived stem cells by microstructured nitinol actuator-mediated mechanical stress. *PLoS One* 2012; 7(12): e51264, http://www.pubmedcentral.nih.gov/articlerender.fcgi?artid=3517541&;tool=pmcentrez&rendertype=abstract (accessed 3 January 2013).
63. Leucht P, Kim J, Wazen R, et al. Effect of mechanical stimuli on skeletal regeneration around implants. *Bone* 2007; 40(4): 919–930, http://www.pubmedcentral.nih.gov/articlerender.fcgi?artid=1987325&;tool=pmcentrez&rendertype=abstract (accessed 11 March 2013).